Acta Materialia 176 (2019) 155–166

Contents lists available at ScienceDirect

Acta Materialia

journal homepage: www.elsevier.com/locate/actamat

Full length article

Deshielding effects on fatigue crack growth in shape memory alloys- A study on CuZnAl single-crystalline materials

Y. Wu [a], J. Yaacoub [a], F. Brenne [a], W. Abuzaid [b], D. Canadinc [c], H. Sehitoglu [a, *]

[a] Department of Mechanical Science and Engineering, University of Illinois at Urbana-Champaign, 1206 W. Green St., Urbana, IL, 61801, USA
[b] Department of Mechanical Engineering, American University of Sharjah, PO Box 26666, Sharjah, United Arab Emirates
[c] Advanced Materials Group (AMG), Department of Mechanical Engineering, Koç University, 34450, Istanbul, Turkey

ARTICLE INFO

Article history:
Received 2 May 2019
Received in revised form
24 June 2019
Accepted 25 June 2019
Available online 27 June 2019

Keywords:
Fatigue crack growth
CuZnAl
Stress intensity factor
Asymmetric phase transformation
Anisotropy

ABSTRACT

The factors that affect the fatigue performance of shape memory alloys (SMAs), including fatigue crack growth (FCG) response, is far from being well-understood. In this study, we point to a mechanism that degrades the FCG performance considerably. We introduce the notion of FCG being affected by shielding and deshielding mechanisms, the former enhancing the resistance while the latter reducing the materials' resistance. We show that the deshielding mechanism creates additional driving forces (positive K contribution) of both Mode II and Mode I types (as much as 5–10 MPa $m^{1/2}$) which accelerates the crack advance. The origin of the positive K component is associated with the localized martensite variant formation that is highly asymmetric with respect to the crack tip. We derive a resultant ΔK in excellent agreement with that measured based on experimental displacement measurements. Overall, this study represents an advancement of our understanding in FCG of SMAs by quantifying the deshielding mechanism.

1. Introduction

1.1. Background

Shape memory alloys (SMAs) are one of the most intriguing materials that have been discovered to date. Their functional properties, i.e. shape memory effect, superelasticity, etc., have been characterized over the years [1,2]. Yet, the explanation of their mechanical response especially under fatigue is still in its infancy [3]. In the presence of cracks, fatigue is a consequence of irreversibility of deformation at crack tips [4]. As a large fraction of the deformation is recovered in SMAs, one must expect a very high fatigue resistance. On the other hand, the experiments typically point to threshold levels and Paris regime behavior which are underwhelming relative to structural materials. For example, the threshold level of NiTi polycrysalline material is 2–3 MPa $m^{1/2}$ [5,6] which falls short of conventional structural materials [7] (4–11 MPa $m^{1/2}$) and other biomedical materials such as non-transforming Ti and Haynes alloys (4–11 MPa $m^{1/2}$) [8]. There has to be some explanation! Of course, one explanation is that even though the recoverability is observed at the macroscale, there are high misfit strains at the austenite-martensite interfaces which lead to irreversibilities [9,10]. Indeed, there is evidence of crack nucleation from a favorable martensite variant/austenite interface followed by crack advance along the interface [11]. We note that as the crack advances, new variants are activated from the crack tip which can carry large shear strains [12]. They can give rise to additional driving forces that are affecting fatigue. But, how large are these driving forces? The current paper is an attempt to understand how these dramatic changes in driving forces can develop in the presence of localized martensite variants.

Earlier and more recent studies on fatigue crack growth in SMAs considered mainly NiTi alloys because of their technological importance [3,5,6,8,13]. The fatigue crack growth resistance of NiTi and the critical stress intensity at fracture could not surpass non-transforming structural materials. Nevertheless, the appearance of crack tip shielding mechanisms has been found to be similar to that of ceramic materials forwarded by McMeeking and Evans [14]. Admittedly, for the NiTi alloys, it is difficult to resolve the variants because the twin plates and the martensite variants accompanying transformation are in nano-dimensions. On the other hand, in CuZnAl [15] such features are more readily visible at macro-scales which allows to pinpoint the localizations associated with

* Corresponding author.
E-mail address: huseyin@illinois.edu (H. Sehitoglu).

https://doi.org/10.1016/j.actamat.2019.06.042
1359-6454/

transformation at the crack tip and measurement of strains (transformation and plastic components) and local displacements. Therefore, the CuZnAl microstructure information is more amenable to quantify. However, it is expected that the fundamental effects can be transferred to any kind of SMA showing formation of martensite confined to variants. A noteworthy difference in CuZnAl compared to other SMAs is its high anisotropic nature of elastic constants and the localization of martensite variants at the macroscale [16]. Therefore, the established fracture mechanics concepts for driving forces found in handbooks [17] need to be modified to account for the geometry of the variants. Such an approach allows the conceptual integration of microscopic variant analysis with macroscopic driving forces. Therefore, the CuZnAl results in this study can constitute a framework for wider application to other SMAs, in general.

1.2. Shielding and deshielding mechanisms

The understanding of crack tip shielding forces in the 1980 and 1990s [18] facilitated the description of fatigue response in many alloys. The effect of plastic zone and transformation zone at the vicinity of a crack tip has been studied in-depth (Fig. 1a). The constraining tractions enveloping the crack reduce the local driving forces [19] imparting crack growth resistance. A myriad of factors affecting the plastic zone and consequently crack growth rates such as the R-ratio, crack size, overload, maximum applied stress, T-stress and notch effects were rationalized based on this approach. Less attention has been devoted to phase transformation effects occurring at the crack tip in fatigue but it has been proposed that the introduction of a transformation zone around the crack produces closure forces and acts as a toughening mechanism. The da/dN - ΔK_{eff} terminology has been often used to denote the intrinsic resistance where ΔK_{eff} parameter is often inferred from experiments. In this paper, the term $\Delta K_{intrinsic}$, is chosen instead of ΔK_{eff} to emphasize essentially the material property nature of crack growth resistance depending on the microstructure and chemical composition. An improvement in da/dN - $\Delta K_{intrinsic}$ resistance is difficult to achieve in reality while the shielding mechanisms can reduce the local driving forces at crack tips and impart an improved extrinsic response as shown schematically in Fig. 1c. The intrinsic stress intensity, $\Delta K_{intrinsic}$, can be represented as the summation of extrinsic stress intensity, $\Delta K_{extrinsic}$, and the change contribution from the transformation zone or plastic zone, ΔK_{change}, at the crack tip, i.e., $\Delta K_{intrinsic} = \Delta K_{extrinsic} + \Delta K_{change}$. $\Delta K_{extrinsic}$ can be interpreted as $\Delta K_{LEFM} = f \cdot \Delta\sigma\sqrt{\pi a}$ and is a function of external stress range, $\Delta\sigma$, crack length, a, and geometric factor, f. ΔK_{change} arises from the tractions on zone surface and it can be negative or positive depending on the shielding (Fig. 1a) or deshielding (Fig. 1b) mechanism. Its calculation procedure is demonstrated in Section 3.3. In this study, we focus on the effect of a transformation zone, i.e. $\Delta K_{transformation}$.

To explain our terminology on shielding better, we note that the $\Delta K_{transformation}$ at crack tip associated with shielding effects is negative (i.e. $\Delta K_{transformation} < 0$). Since $\Delta K_{intrinsic} = \Delta K_{extrinsic} + \Delta K_{transformation}$, the factors that enhance $\Delta K_{transformation}$ (i.e. make it more negative) will have a beneficial role on fatigue crack growth. This means that the da/dN - $\Delta K_{extrinsic}$ curve falls to the right hand side of the da/dN - $\Delta K_{intrinsic}$ curve (Fig. 1c). Since $\Delta K_{extrinsic}$ can be related to $\Delta\sigma$, an improvement in $\Delta K_{extrinsic}$ translates to a higher loading capacity, or higher fatigue resistance. Therefore, the shielding case (such as symmetric transformation configuration) $\Delta K_{extrinsic} > \Delta K_{intrinsic}$ implies an increase in far-field (nominal) loading capacity or increase in fatigue resistance.

On the contrary, and in the case where an asymmetric transformation zone develops around the crack tip, deshielding occurs with positive $\Delta K_{transformation}$ (i.e. $\Delta K_{transformation} > 0$). The notion of deshielding is explained in Fig. 1b and it promotes acceleration of crack growth. Note that in the deshielding case the transformation zone, i.e. the martensite, appears on the upper (or lower) flank of the crack (i.e. one side only without creating an envelope around the crack). Since $\Delta K_{transformation} > 0$ (Fig. 1b), deshielding raises the local stress intensity. Therefore, in this case the $\Delta K_{extrinsic} < \Delta K_{intrinsic}$ which reduces the applied loading capacity or allowable external stress (Fig. 1c). In this case, da/dN - $\Delta K_{extrinsic}$ curve is positioned to the left of the da/dN - $\Delta K_{intrinsic}$ curve, i.e. a decrease in allowable far-field loading. Note that Mode II can contribute to $\Delta K_{transformation}$ in a substantial way depending on the variant and crack orientation (i.e. shearing along the inclined austenite-martensite interface). So variant-induced Mode II implies a further reduction in external load that can be sustained by the material, which translates to a lower loading capacity, or lower

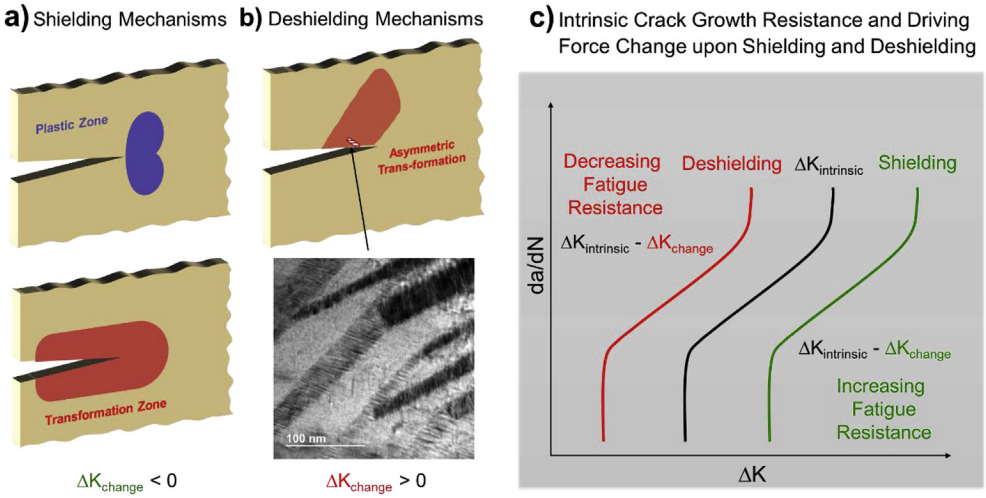

Fig. 1. Summary of (a) shielding and (b) deshielding mechanisms in fatigue crack growth related to transformation and plasticity. In the shielding case (a) there is a reduction of driving force associated with plasticity and symmetric transformation zone while in deshielding case (b) internal tractions elevate the driving force. The deshielding case results in lower crack growth resistance. In (b) TEM results show martensite on only one flank of the crack (c) The da/dN vs. ΔK relationships for a deshielding (red), intrinsic, and shielding (green) cases are demonstrated. (For interpretation of the references to colour in this figure legend, the reader is referred to the Web version of this article.)

fatigue resistance.

The use of digital image correlation (DIC) during a fatigue crack growth experiment enables the extraction of stress intensity factor from the measured displacement fields. This concept was first proposed by McNeill et al. [20]. A least-square regression algorithm was developed by Carroll et al. [21] with the consideration of the T-stress for the accurate ΔK_I determination in an isotropic case. It was further extended to an anisotropic mix mode case by Pataky et al. [22]. Such a K-extraction algorithm was successfully applied on SMAs to find both ΔK_I and ΔK_{II} values [13,16]. Since these measured DIC displacements directly reflect the crack growth nature of the material, the extracted stress intensity can be interpreted as the effective value or $\Delta K_{intrinsic}$.

The modification of the crack tip driving forces due to localized transformation zones has been recognized in transforming materials in the 1980s. For example, in ceramic material, McMeeking and Evans [14] demonstrated that the tractions on an inelastic domain can effectively affect the stress intensity at the crack tip. These tractions can be evaluated using Eshelby's inclusion method [23] and the stress intensity arisen from these tractions ($\Delta K_{transformation}$) can be further calculated using weight function theory [24]. They showed that the crack tip driving force can be reduced by the presence of these surface tractions, i.e. $\Delta K_{transformation} < 0$, providing toughening or shielding effect. An anisotropic analysis was developed in our previous study for Ni_2FeGa and NiTi SMAs [16] in Mode I, which also showed reduction in crack tip driving force. In this study, we demonstrate the calculation of $\Delta K_{transformation}$ in a mixed-mode scenario of CuZnAl which has an asymmetric transformation behavior.

1.3. Symmetric vs. asymmetric transformation

When scrutinizing the previous studies, we note that the transformation behaviors of Ni_2FeGa [16] and NiTi [25] are observed to be symmetric where the transformation domain exhibits a mirror symmetry with respect to the crack plane. For CuZnAl on the other hand, the experimental evidence indicates that the transformation zones both ahead and in crack wake are highly asymmetric. This occurs because martensite localization due to variant selection could occur in view of the anisotropy and complex stress states at the crack tip [11]. We note that high elastic anisotropy in CuZnAl renders the crack tip stress fields a strong function of polar angle biasing one variant in favor of others. The non-symmetric tractions in the crack wake can produce completely different driving forces and undoubtedly accelerating the crack growth. The possibility of internal forces increasing the driving forces due to such asymmetric transformation response, i.e. producing deshielding effects as discussed above, has not been elucidated in past studies. In this paper, we address this hypothesis utilizing CuZnAl single crystals as an example alloy. The change in crack tip driving force is determined, in terms of the stress intensity arisen from the internal tractions on transformation zone, to be substantial (near 5–10 MPa $m^{1/2}$).

In earlier studies, the calculation of the driving force modification has been confined to Mode I component due to a flat crack configuration developed within the materials, especially in NiTi. The flat crack geometry can result from the activation of multiple variants [16]. On the other hand, in Cu-based SMAs the variant selection depends on the local stress state and a single variant is often favored. Since the threshold levels in many of the SMAs are in the range from 2 to 10 MPa $m^{1/2}$ [5,13,16,26], the transformation induced stress intensity changes exceeding 5 MPa $m^{1/2}$ could have a profound effect on the threshold resistance. In particular, the Mode II component can be substantial even though the crack inclination is small and the external stress is tensile.

In summary, this paper is concerned with the determination of fatigue crack growth driving forces in the presence of localized martensite variants in SMAs. The stress field induced from localized transformation are determined utilizing Eshelby's equivalent inclusion and weight functions incorporating shear and normal tractions and their interaction. A schematic that delineates the change of a crack tip driving force due to an asymmetric transformation zone is illustrated in Fig. 2 where Ω denotes the transformation zone and D-Ω the untransformed region. Based on the simulations we can confirm the role of the transformation dimensions, i.e. crack length (a) and zone height (w), and show that the effective stress intensity depends on the elastic constants associated with the autensite, C_{ijkl}, and martensite, C'_{ijkl}, and the magnitude of the equivalent eigenstrain, ε^{**}_{kl}.

2. Material and experimental methods

In this study, we use single crystal CuZnAl SMAs to eliminate complications arising from grain boundaries. Still, as described above for other SMAs, the fundamental mechanism is seen to be effective in polycrystals as well, giving the formation of martensite variants is asymmetric with respect to the crack tip. The nominal composition of the selected material is $Cu_{72.61}Zn_{20.64}Al_{5.98}$ (at.%) with 0.41 at.% of Co. The slab was sectioned into dog-bone specimens with a gauge area of ~3 mm × 10 mm and 1.5 mm thickness. All specimens were heated treated at 800 °C for 30 min followed by water quenching and ensued with an aging treatment at 80 °C for 24 h. After the heat treatment, the specimens were mechanically polished to a mirror finishing using abrasive papers (400–1800 grits). From electron backscattering diffraction (EBSD) analysis, the loading direction was determined as [0.191 0.811 0.553] which is

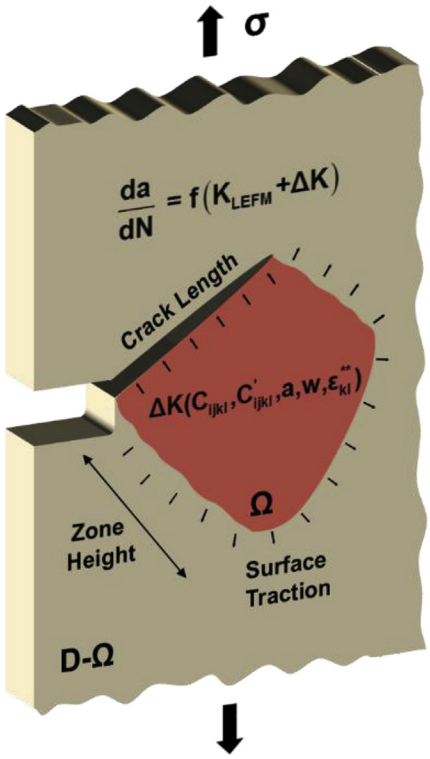

Fig. 2. A schematic illustrating the increase of crack tip driving force due to an asymmetric transformation behavior of a slanted crack. The transformation induced stress intensity factor can be a function of Austenite/Martensite elastic constants (C_{ijkl}/C'_{ijkl}), crack length (a), zone height (w) and equivalent eigenstrain (ε^{**}_{kl}).

close to [143] orientation. Hence, the single crystal will be designated as [143] CuZnAl thereafter. A speckle pattern was later airbrushed onto the specimen surface for digital image correlation strain analysis (DIC). The details about DIC can be found elsewhere [27]. Tension experiments were conducted using a servohydraulic load frame, in displacement control, with a rate of ~0.003 mm/s and was unloaded in stress control. Optical images of the gauge section were captured, in-situ, during loading and unloading for DIC measurements. The resulting stress-strain response is shown in Fig. 3. In addition, tension-tension fatigue crack growth experiment was performed on a [143] CuZnAl single crystal dog-bone sample with a 0.5 mm deep notch cut in the middle of the gauge section. The maximum stress level was approximately 45 MPa and the minimum 2.25 MPa, which corresponds to an R ratio of 0.05. The sample was cycled at 3 Hz, however during measurement cycles, the frequency was reduced to 1 Hz to capture as many images as possible in one loading and unloading cycle. Measurement cycles were conducted once every 500 cycles upon the nucleation of a fatigue crack from the machined notch. The displacement fields obtained from the measurement cycles using DIC were later fit to the analytical solution to determine the effective (intrinsic) stress intensity factor range. Subsequent to the fatigue crack growth tests, microstructural analysis of the transformation zone was conducted by transmission electron microscopy (TEM). Bright-field images and diffraction pattern were obtained using a JEOL 2100 Cryo TEM operating at 200 kV. The corresponding specimens were extracted in direct vicinity to the crack (see Fig. 5e) using focused ion beam (Thermo Scios2 Dual-beam SEM/FIB).

3. Experimental and modeling results

In this paper, we analyze an inclined crack subjected to remote tensile loading. In Section 3.1, the superelastic behavior and crystal orientation of the sample are presented and confirmed using EBSD. The strain contours before and after crack initiation are demonstrated in Section 3.2. We believe that the engendered transformation domain can be attributed to the creation of two important interfaces (two different martensitic variants), the first associated with transformation ahead of the notch and the second with transformation ahead of the initiated crack. The first interface corresponds to the martensite emanating from the notch. This interface has a major influence on the orientation of the initiated crack which forms along the austenite to martensite variant interface and is oblique to the notch. Once the crack forms, it proceeds to grow along the preferred variant. However, more importantly, as the crack grows, it results in an activation of a new variant (second interface) that is most favorable in view of crack tip stress fields. The calculation for the stress intensity associated with the tractions on the transformation zone surfaces is showcased in Section 3.3. The formulations allow rapid assessment of the stress intensity factors. It utilizes weight functions that are general and uses expressions for deriving both the Mode I and Mode II components. The sensitivity of such calculation due to the variations of several parameters are illustrated in Section 3.5. In Section 3.4, the K values calculated from classical LEFM, regression fitting to the cubic anisotropic displacement solutions and the corrected LEFM values with the K due to transformation (current study) are presented and compared.

3.1. Superelasticity of [143] CuZnAl at room temperature

Fig. 3a illustrates the superelastic response of [143] CuZnAl alloy at room temperature in tension. In this case, the critical transformation stress level reaches ~50 MPa (0.2% offset). Prior to the deformation, the orientation of the single crystal was confirmed using EBSD. The results are shown in Fig. 3b. The loading orientation (Y) was found to be [0.191 0.811 0.553] ~ [143], transverse direction (X) [0.900 -0.368 0.231] ~ $[9\bar{3}1]$, and normal direction (Z) [-0.391 -0.454 0.800].

3.2. Crack tip strain field and transformation zone microstructure

Fig. 4a illustrates the DIC strain contour at the pre-cracking stage (i.e. notch only, no fatigue crack). It is evident that two strain localization bands are emanated from the notch tip and the upper one is more dominant. The angle of the upper band is approximately 39° and it is identified via trace analysis as (−0.669 -0.182 -0.721)[0.737 -0.165 -0.655] type of martensitic variant (V17) based on the habit plane normal and transformation shear direction reported by Patoor et al. [28]. The corresponding Schmid factor is 0.43, which is also the highest among the 24 possible variants. Fig. 4b demonstrates the DIC strain contours post crack initiation when the crack length is roughly 1.05 mm. Note that the crack angle illustrated in Fig. 4b complies with that of the V17 projection in Fig. 4a (prior to crack initiation). As a result, we believe that the crack nucleates at the interface between austenite and martensite. Fig. 4b demonstrates the strain contour at the maximum load. Additional TEM analysis will help to identify the martensitic

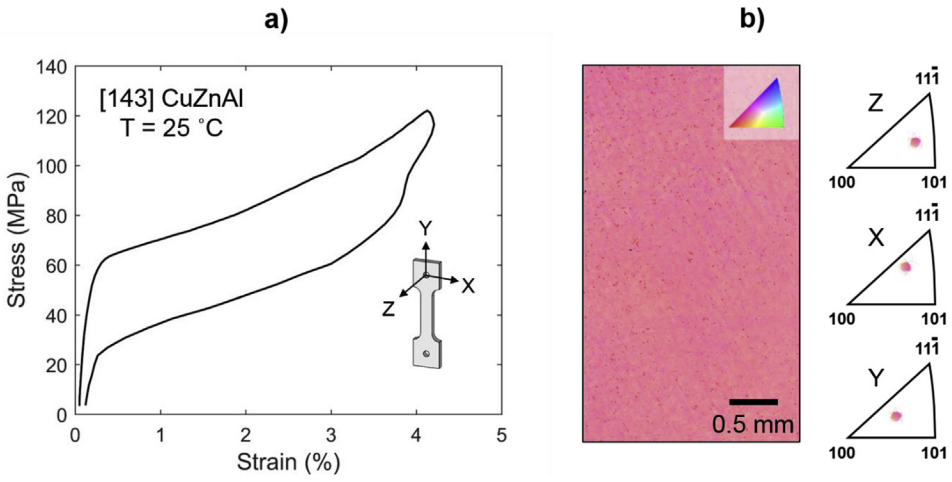

Fig. 3. a) The stress-strain behavior of [143] CuZnAl single crystal and b) the EBSD map confirms the orientation of the single crystal.

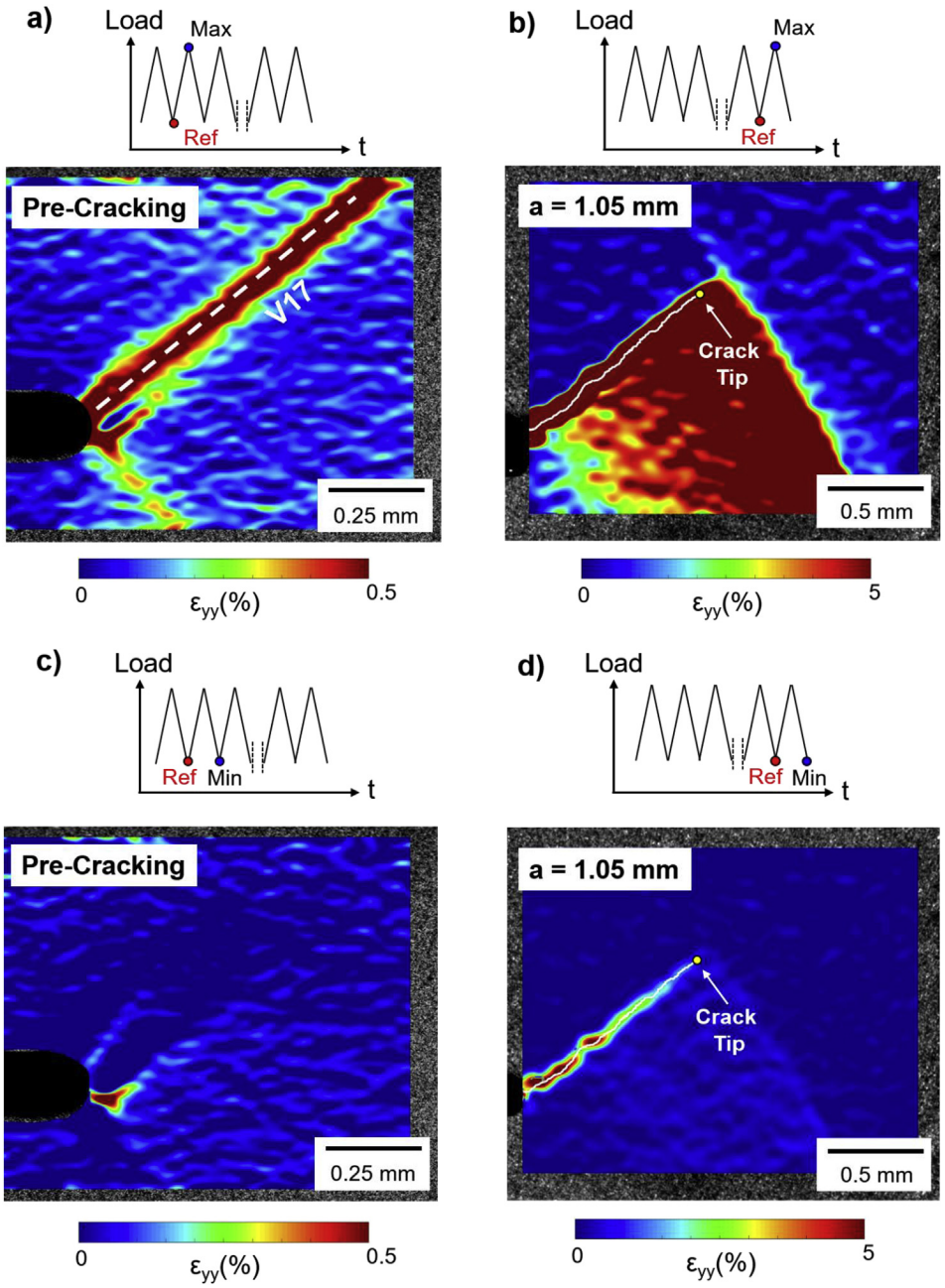

Fig. 4. The strain contours of a) the maximum load level at the pre-cracking stage, b) the maximum load level post-cracking (a = 1.05 mm), c) the minimum load at the pre-cracking stage and d) the minimum load level at a longer crack (a = 1.05 mm).

variants activated in the strain localized area. To calculate $\Delta K_{transformation}$, the transformation zone is idealized as a rectangular shape in Section 3.3. The strain contours at the minimum stress levels are presented in Fig. 4c and d for the pre-cracking and cracked cases after 10000 cycles, respectively. We observed that low residual strains are present within the transformation zone only.

Formation of martensite in course of crack initiation and growth was confirmed by TEM analyses of the [143] sample after 10000 cycles. Fig. 5a the variants are identified as V2 (−0.669 -0.182 -0.721)[0.737 -0.165 -0.655] and V17 by trace analysis of the TEM specimen. Fig. 5 (b) clearly shows the internally twinned structure of V17, leading to the typical diffraction pattern of the M18R martensite structure (Fig. 5b1), as also shown in e.g. Ref. [29]. The diffraction pattern of the austenitic matrix (DO_3) is given in Fig. 5b2 for comparison. In light of the superelastic behavior (Fig. 3a) and the low residual strains (Fig. 4), the presence of martensite upon unloading might be surprising. However, martensite stabilization is typically observed under cyclic load and attributed to high dislocation activity, leading to pinning of martensite variants formed upon exceeding the corresponding critical stresses at high load levels [30,31]. A high dislocation activity within the transformation zone is confirmed in Fig. 5c in form of diverse slip bands within the austenitic matrix. The enlargement in Fig. 5d shows the close interaction between these slip bands and the V2 martensite, leading to stabilization and presence of martensite upon unloading. Fig. 5e illustrates the position of the TEM lamella extracted relative to the crack. The lamella was then investigated from the side as shown in the schematic as an inset in Fig. 5e.

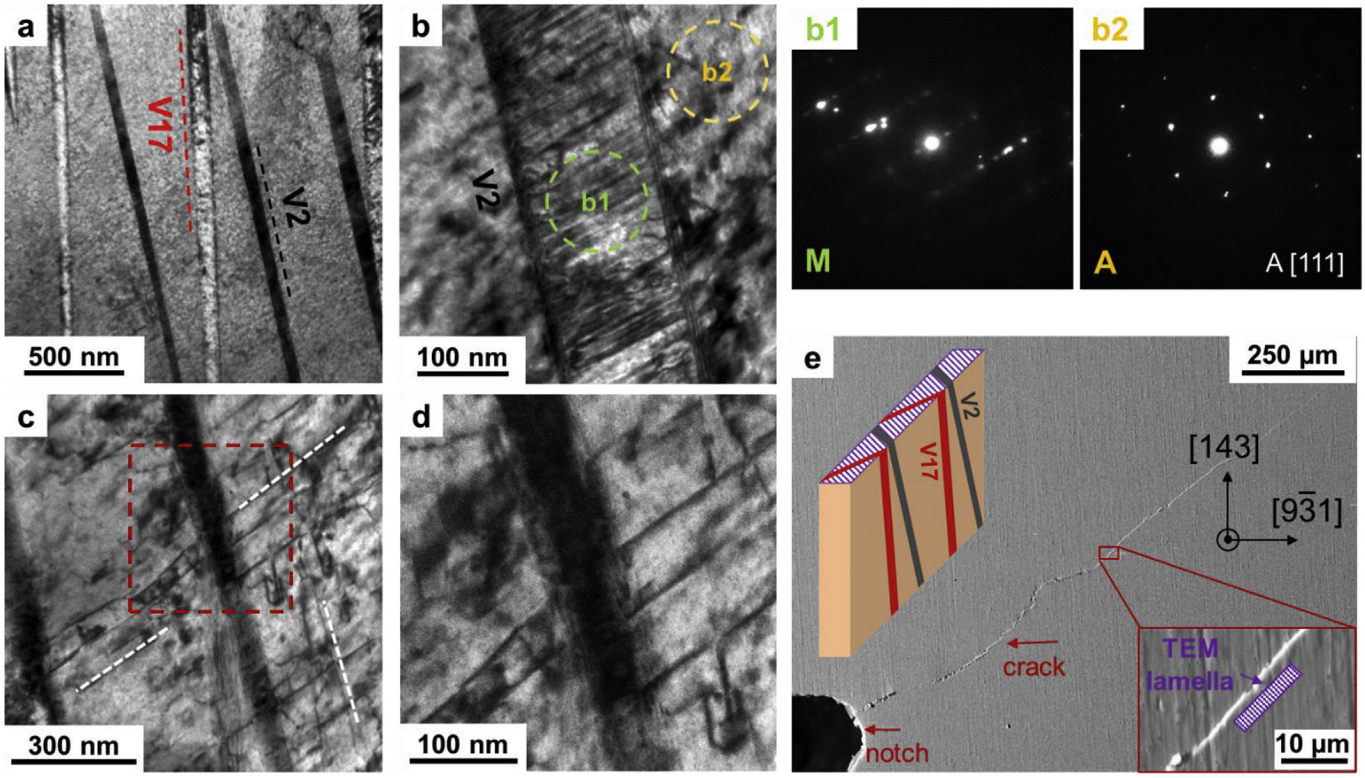

Fig. 5. a) TEM bright-field image showing V2 and V17 type of martensite within the austenitic matrix. (b) V17 martensite at high magnification highlighting internally twinned nature and corresponding SAED pattern of (b1) V17 martensite and (b2) the austenitic matrix on [111] zone axis stemming from the area indicated by the dashed circles in (b). (c) TEM bright-field image obtained at different tilting angle showing multiple glide bands as highlighted by the dashed lines within the austenitic matrix. (d) higher magnification of the area marked by the dashed square in (c) indicating pinning of martensite by dislocation glide in direct vicinity of the formed variant. (e) scanning electron microscopic image showing the site of TEM specimen extraction relative to the crack. The TEM lamella was investigated from the side as shown in the inset. The loading and transverse directions are shown as well.

3.3. *The determination of $\Delta K_{transformation}$ ascribed to the transformation behavior in the case of deshielding*

The driving force of the crack propagation in CuZnAl SMAs can be effectively modified by the tractions on the transformation zone surface present behind the crack tip. Such $\Delta K_{transformation}$ due to the non-symmetric transformation is numerically determined in this study (i.e. deshielding case). The calculation utilizes the internal stress and strain fields within the transformation zone and the weight function theory to obtain the relevant $\Delta K_I^{transformation}$(Mode I) and $\Delta K_{II}^{transformation}$(Mode II) values due to the traction fields on different zone surfaces. The calculation procedure resembles that presented in Wu et al. [16], but the current study considers both Mode I and Mode II components. A schematic is shown in Fig. 6 to elucidate the points, where a denotes the crack length, w is the zone height, t_i represents the surface traction, 'θ is the crack angle, xyz is the crystal frame, and x'y'z' is the crack frame.

By treating the transforming zone as an inclusion, we can compute the internal strain level using Eshelby's equivalent inclusion method. The corresponding equivalent eigenstrain can be calculated from the strain fields measured via DIC that are illustrated in Fig. 4. The DIC strain can be interpreted as the total strain, ε_{ij}^{tot}, including both constrained strain, ε_{ij}^{c}, and far field strain, ε_{ij}^{far}. Therefore, the intrinsic transformation strain, ε_{ij}^{p}, can be calculated as follows,

$$\varepsilon_{ij}^{p} = S_{ijkl}^{-1}\left(\varepsilon_{kl}^{tot} - \varepsilon_{kl}^{far}\right) \tag{1}$$

whereS_{ijkl} is the Eshelby's tensor for cubic material and its definition can be found in Ref. [32]. When an external load is applied, both the eigenstrain associated with the modulus mismatch between austenite and martensite, ε_{ij}^{*}, and the ε_{ij}^{p} need to be taken into account. The sum of ε_{ij}^{*} and ε_{ij}^{p} is also known as equivalent eigenstrain, ε_{ij}^{**}, and it can be calculated using Equation (2) [32],

$$C_{ijkl}\left(\varepsilon_{kl}^{far} + S_{klmn}\varepsilon_{mn}^{**} - \varepsilon_{kl}^{**}\right) = C_{ijkl}^{'}\left(\varepsilon_{kl}^{far} + S_{klmn}\varepsilon_{mn}^{**} - \varepsilon_{kl}^{p}\right) \tag{2}$$

where C_{ijkl} is the elastic constants of the austenite and $C_{ijkl}^{'}$ is the elastic constants of the martensite. The elastic constants of CuZnAl were previously determined using density functional theory (DFT) and were reported in Wu et al. [16]. The internal stress field, σ_{ij}, in the transformation zone can be calculated as the follows [14,33],

$$\sigma_{ij} = C_{ijkl}\varepsilon_{kl}^{**} \tag{3}$$

After rotating the stress field from the crystal frame (xyz) to crack frame (x'y'z') via a simple transformation matrix, $\sigma_{ij}^{'} = Q_{im}Q_{in}\sigma_{mn}$, where Q is the transformation matrix, the tractions can be achieved via Equation (4),

$$t_i^{'} = n_j^{'}\sigma_{ij}^{'} \tag{4}$$

where $n_i^{'}$ is the outward normal vector of the transformation zone in x'y'z' coordinate frame. Upon acquiring the surface tractions, it is feasible to compute the corresponding $\Delta K_I^{transformation}$and $\Delta K_{II}^{transformation}$values using the weight function methodology forwarded by Bueckner [34] and Rice [24]. The expressions of $\Delta K_I^{transformation}$ and $\Delta K_{II}^{transformation}$ due to internal tractions are

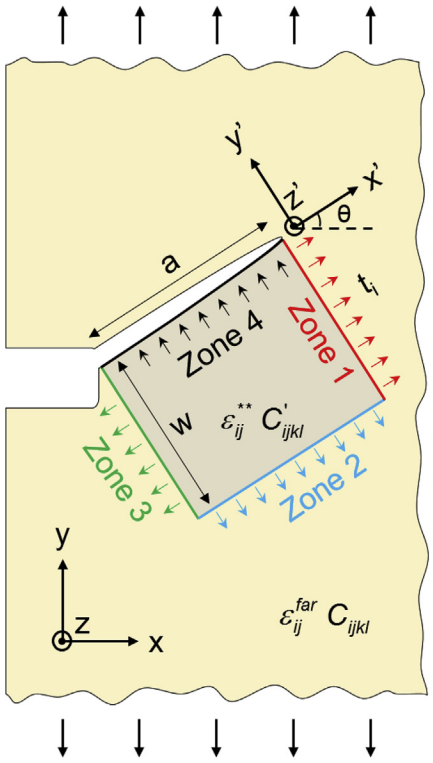

Fig. 6. A schematic illustrates the loading systems of the asymmetric transformation zone surfaces. In this study, the transformation zone is approximated as a rectangular shape. It was further divided into four sections (Zones 1, 2, 3 and 4), where a denotes the crack length and w the zone height. The K values were calculated from each zone and the combination of the K values yields the net change of K arisen from the transformation behavior. We found both Mode I and Mode II yield positive K values, which leads to deshielding in CuZnAl.

Table 1
Stress intensity factors associated with the surface tractions imposed on different zone boundaries are calculated and the results are tabulated below when the crack length is roughly 0.95 mm. The calculation was performed at the maximum load level (45 MPa) and assuming w/a = 1.

Zone #	$\Delta K_I^{transformation}$	$\Delta K_{II}^{transformation}$
	MPa$\sqrt{m}$	
1	3.32	0.65
2	−0.62	−1.72
3	4.37	2.77
4	−2.85	3.78
Total	4.22	5.48

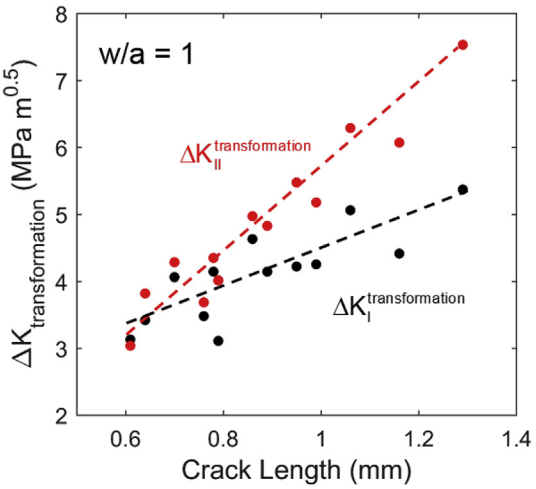

Fig. 7. The evolution of $\Delta K_I^{transformation}$ and $\Delta K_{II}^{transformation}$ as a function of the crack length.

shown in Equation (5),

$$\Delta K_I^{transformation} = \int_{S_p} (t_{x'} h_{Ix'} + t_{y'} h_{Iy'}) dS_p \quad (5a)$$

$$\Delta K_{II}^{transformation} = \int_{S_p} (t_{x'} h_{IIx'} + t_{y'} h_{IIy'}) dS_p \quad (5b)$$

where $h_{x'}$ and $h_{y'}$ are the anisotropic weight functions which are further derived in the Appendix and dS_p is the line element of the zone perimeter. Note that the presence of horizontal tractions affects both Mode I and II components. The derivation of the weight functions is elaborated in the Appendix.

The $\Delta K_I^{transformation}$ and $\Delta K_{II}^{transformation}$ values of each zone are tabulated in Table 1, when the crack length is approximately 0.95 mm and the w/a ratio is set to be 1. Note that the contribution from Zone 2 is slightly lower while those from Zones 1, 3 and 4 are relatively substantial. The evolution of $\Delta K_I^{transformation}$ and $\Delta K_{II}^{transformation}$ as a function of crack length is demonstrated in Fig. 7. It is important to mention that each point was calculated from the DIC strain field extracted from the transformation zone of that specific crack length. From Fig. 7, we note that the K modification in Mode II is slightly higher than that in Mode I especially at longer crack when w/a = 1.

We draw attention to the increasing change in K as the crack gets longer in Fig. 7 which is indicative of a crack-size dependent behavior. The increase in local driving forces are predominantly due to crack wake effects; yet we note that even when the crack wake is small, the change in K is evaluated in the vicinity of 3 MPa m$^{1/2}$ which is substantial. Such a magnitude of $\Delta K_{transformation}$ completely alters the extrinsic threshold stress intensity values.

3.4. Fatigue crack growth behavior of [143] CuZnAl

The effective stress intensity factor can be obtained by regression fitting the experimental DIC displacement field to the anisotropic displacement fields for cubic crystals. Such procedure has been explained in many previous studies for both transforming [13,16] and non-transforming materials [21,22]. The comparisons between the theoretical and experimental (from DIC measurements) displacement fields are demonstrated in Fig. 8a and c for a short 0.5 mm crack (Point A) and a 1.5 mm long crack (Point B), respectively. Note that a good agreement between theoretical and experimental results is evident and it is consistent throughout our analyses. From the vertical and horizontal displacements, we can obtain $\Delta K_I^{regression}$ and $\Delta K_{II}^{regression}$ which are the Mode I and Mode II component, respectively. The total $\Delta K_{regression}$ can be calculated as follows [35],

$$\Delta K_{regression} = \sqrt{\left(\Delta K_I^{regression}\right)^2 + \alpha\left(\Delta K_{II}^{regression}\right)^2} \quad (6)$$

where α is the ratio between energy release rates associated with Mode I and Mode II, J_2/J_1, as shown in Equation (7).

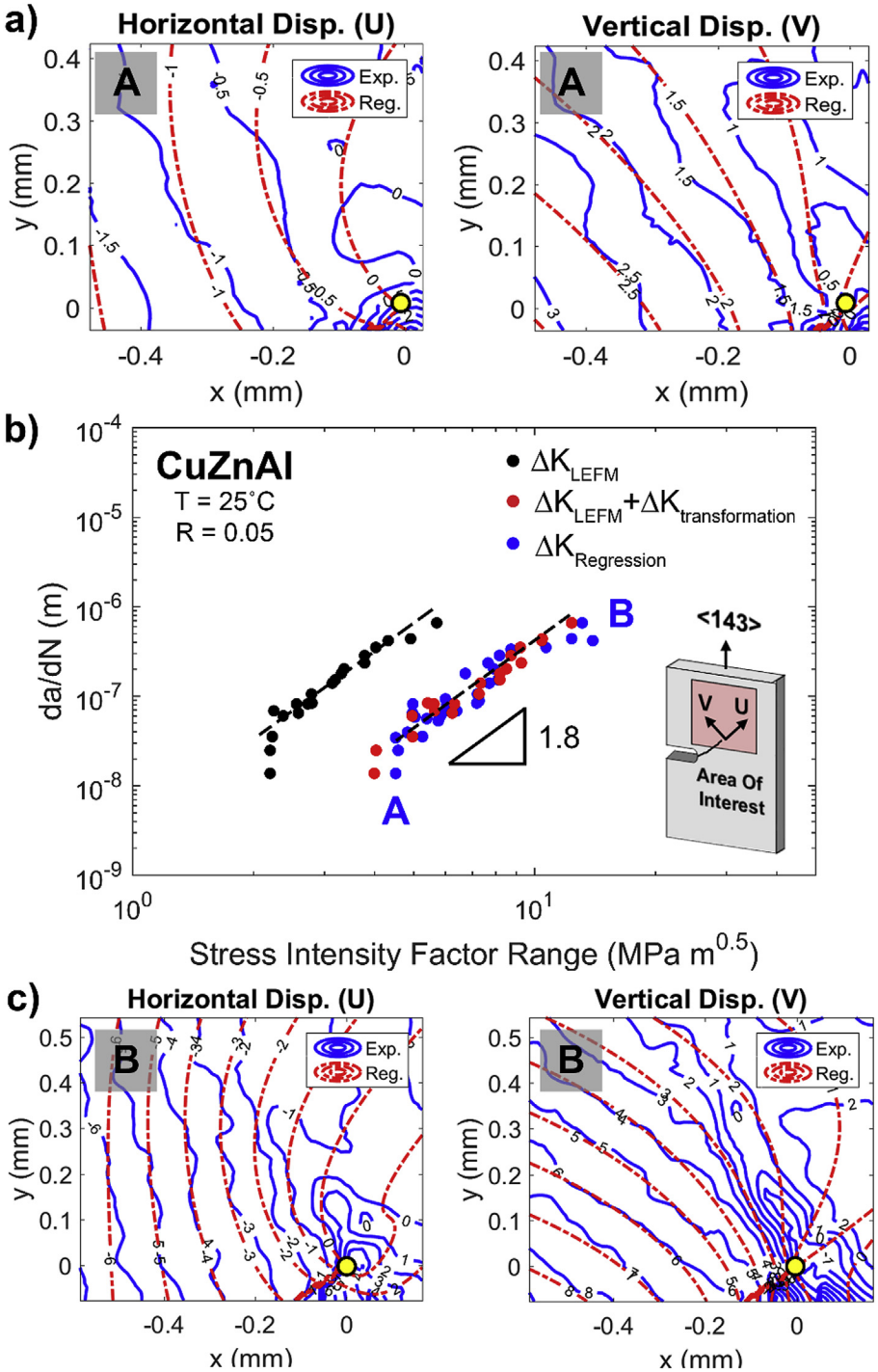

Fig. 8. a) The regression results are illustrated for both horizontal and vertical displacement fields at Point A where the crack length is roughly 0.5 mm. The crack tip is highlighted with a yellow dot. b) The crack growth rate (da/dN) is plotted against the stress intensity factor range. The black dots demonstrate the results from the handbook (LEFM), blue dots the regression results, and the red dots are the combination of handbook results and the calculated $\Delta K_{transformation}$. Note that this is a deshielding case with $\Delta K_{transformation}$ near 4 MPa $m^{1/2}$. The intrinsic threshold is near 5 MPa $m^{1/2}$. The dashed lines are added to aid the eye. c) The regression results are illustrated for both horizontal and vertical displacement fields at Point B where the crack length is roughly 1.5 mm. (For interpretation of the references to colour in this figure legend, the reader is referred to the Web version of this article.)

$$J_1 = -\frac{\pi K_I}{2} a_{22} \mathrm{Im}\left[\frac{K_I(\mu_1+\mu_2)+K_{II}}{\mu_1\mu_2}\right] \tag{7a}$$

$$J_2 = \frac{\pi K_{II}}{2} a_{11} \mathrm{Im}[K_{II}(\mu_1+\mu_2)+K_I\mu_1\mu_2] \tag{7b}$$

The correlation between crack growth rate (da/dN) and stress intensity factor ranges is illustrated in Fig. 8b. The blue dots represent the $\Delta K_{regression}$ values acquired from regression fitting. Note that the effective threshold value is close to 4.5 MPa $m^{1/2}$ for [143] CuZnAl which is lower than superelastic Ni_2FeGa (~8 MPa $m^{1/2}$) [16] and higher than stable austenitic NiTi (~1.5 MPa $m^{1/2}$) and

martensitic NiTi (~2.1 MPa $m^{1/2}$) [13]. The slope of the Paris region (Stage II) is approximately 1.8. The black dots are the ΔK_{LEFM} values obtained from the handbook solution by Tada, Paris and Irwin [17] for a slanted crack. We found that the ΔK_{LEFM} values fall significantly short of $\Delta K_{regression}$. After considering the change of the crack tip driving force due to asymmetric transformation by incorporating ΔK_{LEFM} with $\Delta K_{transformation}$ (shown in Figure (6)), i.e. $\sqrt{(\Delta K_I^{LEFM} + \Delta K_I^{transformation})^2 + \alpha(\Delta K_{II}^{LEFM} + \Delta K_{II}^{transformation})^2}$ (red dots), the results match with each other very well.

3.5. The sensitivity of $\Delta K_{transformation}$ calculation

In this section, we present the sensitivity of $\Delta K_{transformation}$ values due to the variations in relevant parameters, such as w/a ratio, $C_{ijkl}\epsilon_{ij}^{**}$, etc. Fig. 9a illustrates the evolution of $\Delta K_{transformation}$ values as a function of the geometric parameter (w/a) while keeping the other factors constant. Note that both $\Delta K_I^{transformation}$ and $\Delta K_{II}^{transformation}$ increase with the increase of w/a, while the former grows faster than the latter. Nevertheless, the magnitude of the Mode II component remains substantial. Fig. 9b and c demonstrate the influence of C_{ijkl} and ϵ_{ij}^{**} on $\Delta K_{transformation}$: the $\Delta K_{transformation}$ values also increase with increasing magnitude of C_{ijkl} and ϵ_{ij}^{**}.

4. Discussion of results

The role of the localized transformation zones that are non-symmetric is to introduce an additional stress intensity component (i.e. $\Delta K_{transformation} > 0$) which causes deshielding and degradation in fatigue crack growth resistance. In the case of the martensite variants in this work, we note the presence of a substantial Mode II stress intensity component. Considering the notion that the intrinsic resistance such as the threshold stress intensity value is a material property, akin to friction stress for example, we make the following argument. The stress intensity experienced by the crack has two components: one due to applied loading and the other is due to internal tractions. If the internal tractions provide a positive K term then the net effect is a reduction in the allowable applied K component. This effectively reduces the allowable external stress. On the other hand, if the internal forces provided a negative K contribution then the effect of this is to allow a higher applied K component, which can be viewed as shielding mechanism, such as observed in Ni_2FeGa [16]. The negative contribution is well-known in transformation studies which emanates from compressive tractions at the crack flanks. On the other hand, the upshot of a positive contribution on the driving forces is less understood but can be significant. Therefore, we point to the categorization of SMAs into two categories: shielding versus deshielding controlled fatigue crack growth. While the shielding effect is well conceived in the literature [16,25,33], the possible deshielding effect is much less elucidated.

Based on our experimental results so far, the CuZnAl (this study) and FeMnNiAl (unpublished) both exhibit deshielding behavior while NiTi and Ni_2FeGa display shielding response. The CuZnAl system has a much higher anisotropy, compared to NiTi, while FeMnNiAl has a smaller number of lattice correspondences, (3) compared to NiTi (12). Although the deshielding mechanisms and causes are still under study, the phenomenon can be attributed to the aforementioned factors for CuZnAl ((i) the anisotropy of elastic constants) and FeMnNiAl ((ii) the number of lattice correspondences). Other factors can also have a contribution including: (iii) local crystal orientation and stress state and (iv) latent hardening which affects the transformation variants in latent systems due to variant activation in the main system would also have an effect.

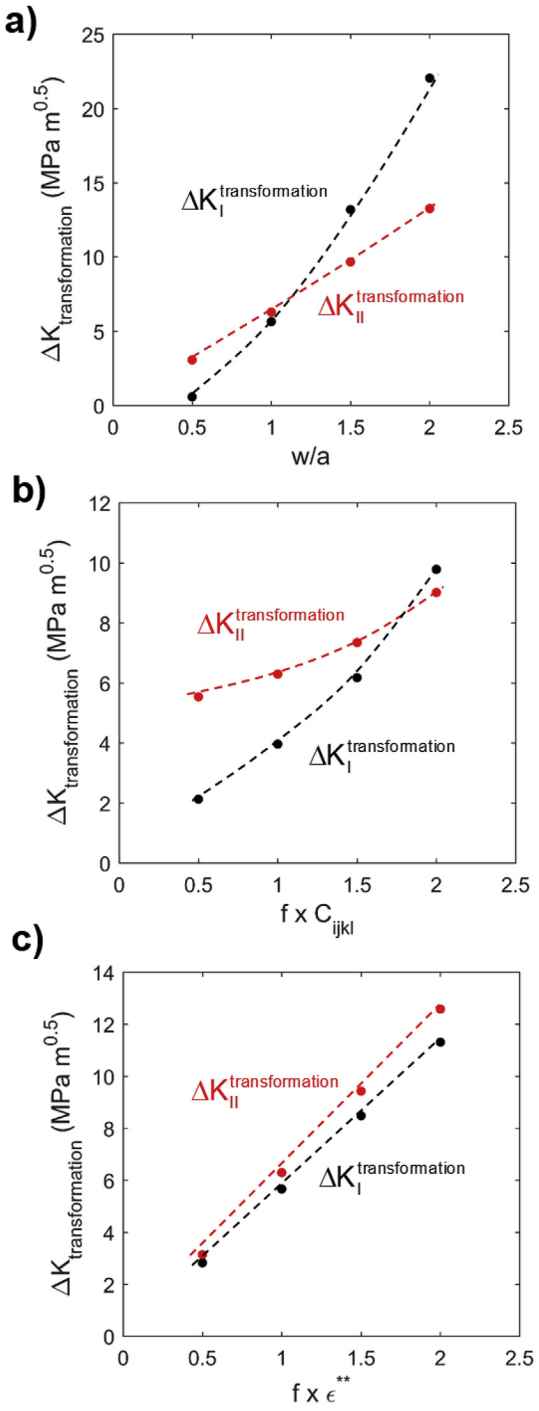

Fig. 9. The sensitivity of the $\Delta K_{transformation}$ values due to the variation of three parameters: a) w/a, b) C_{ijkl} and c) ϵ^{**}. The factor f (which is plotted as x-axis) is in the range 0.5–2.

Among the factors above, items (i) and (ii) are expected to have the largest effects as evident from the experimental results.

The present results develop the notion of a deshielding mechanism which can be utilized in conjunction with the Paris law representation of fatigue crack growth [5,13,16,26] to gain a true intrinsic crack growth resistance. In some SMAs, the transformation zone is symmetric, i.e. NiTi and Ni_2FeGa, while in others, i.e. CuZnAl and FeMnNiAl the variant localization transpires at one side of the crack. The shape of the transformation zone in general can be even more complex. Even in polycrystals, near the threshold regime, the

role of microstructure and the localized transformation variants are expected to produce variations from the conventional stress intensity descriptions and modeling efforts shown in this study will prove to be extremely useful. Therefore, the findings in this paper are an attempt to improve the understanding of fatigue crack growth behavior in SMAs.

We note that volume changes, which are pronounced during transformation in ceramics, can indeed be present in some SMAs as well. For example, the CoNiAl and NiFeGa SMAs exhibit finite positive and negative volume changes respectively compared to NiTi which undergoes a small negative volume change [36]. Our formulation would accommodate the volume change effects readily. In the case of SMAs such as CuZnAl, the volumetric strains are near zero [12] while the transformation shear strains are much larger and dominate. When the transformation zone is symmetric, then the transformation shear is resolved to strains normal to crack plane and corresponding negative tractions surrounding the crack wake shield the crack. However, if the transformation zone is asymmetric, the transformation shear adds a large shear driving force as noted in this paper. Such a shear contribution to stress intensity does not exist for the symmetric case. It is this additional shear driving force that limits the fatigue crack growth resistance in a number of SMAs.

We also point to the ease of measurement of transformation zones via strain measurements in CuZnAl (this study) and FeMnNiAl at macroscales [37]. On the other hand, it is possible that the presence of localization may not be readily viewed in optical microscopy or with digital image correlation [38] because the martensite variants are extremely fine in NiTi for example [39]. Nevertheless, when such variants are asymmetric with respect to the crack tip in view of the high elastic anisotropy and the prevailing stress states, then the deshielding effects dominate. In similar fashion, this mechanism can be transferred from the single crystal material contemplated in the current study to polycrystal material. However, as stated in the manuscript additional complications stemming from grain boundaries had to be avoided for these fundamental investigations, which is why a CuZnAl single crystal was investigated.

We also make the following remark on the fatigue crack growth resistances of stable austenite vs martensite have been studied in past research studies. It was found that the martensite exhibits superior resistance as shown by Ritchie on polycrstalline NiTi [5] and by Sehitoglu et al. on single crystalline NiTi [13]. These previous experiments were conducted in the purely martensitic regime and purely austenitic regime (i.e. stable austenite, no transformation) and the fatigue crack growth results were compared. In the case of austenite to martensite transformation as in this study, the crack tip crystal structure alternates between austenite and martensite during a fatigue cycle and the driving forces and fatigue crack growth rates are mainly governed by the tractions induced by the transformation strain. Consequently, we emphasize that the fatigue crack growth response will depend on the elastic moduli difference, the anisotropy of austenite and martensite, the transformation strain tensor, the propensity of plastic flow and martensite variant location including its boundaries and inclination as described in this study. Future studies must consider the response of CuZnAl in the stable austenite and martensite regimes to gain further insight on the monolithic response.

We note that although no gross plastic deformation takes place (strain almost completely recovers upon unloading in the transformation zone as shown in Fig. 4c), the results are affected by a degree of irreversibility in strain that develops at within the transformation zone. An important consideration for crack growth analysis is the resistance to plastic flow to minimize the irreversible strains. Since these materials do not obey the Schmid Law [40], the nucleation and crack growth would also be affected by the plastic flow resistance. In our supplementary TEM work in the transformation zone in CuZnAl, the presence of plastic deformation is evident. However, detailed analysis of phenomena related to plastic flow is outside the scope of the current study and is left for future studies.

One of the major findings of this study is the recognition of the fact that the development of asymmetric transformation field in the vicinity of an advancing fatigue crack causes deshielding, which adversely affects the fatigue crack growth response. Another point in this paper is the role of asymmetric tractions producing a high Mode II contribution to fatigue crack growth. Finally, we would like to point that this is a very comprehensive study because thousands of material points are tracked and used to derive an intrinsic stress intensity factor so that we can make a demarcation between the extrinsic and intrinsic values. In addition to the presented results, we observed the asymmetric transformation zones in [001] and [011] CuZnAl single crystals [43] and also in FeMnNiAl single crystals(not reported here). Future studies should make digital image correlation observations at high magnifications with loading stages inside scanning or transmission electron microscopes to observe variants which may have submicron dimensions in certain shape memory alloys.

In summary, we are able to explain the contrasting behavior of SMAs that exhibit shielding and deshielding effects. We evaluate the stress intensity utilizing two methods: (a) fitting the displacements fields to the analytical anisotropic displacement solutions by performing a least-squares regression and (b) handbook solutions for stress intensity corrected with stress intensity due to internal tractions around non-symmetric transformation zones. Both methods gave the same result which increases the confidence level in our methodology. The fracture mechanics hand book K-solution falls far short of the regression solution, the difference being the deshielding term. The results not only explain the local driving forces for accelerated crack growth in SMAs with non-symmetric transformation, but also provides a framework for calculating the intrinsic (i.e. effective) K values. It is noted that such behavior is not unique to Cu based SMAs and is expected to dominate in other SMAs especially near the threshold regime where local variant effects dominate.

5. Conclusion

We draw the following conclusions from the current study:

(i) Unlike NiTi where a symmetric transformation pattern develops near the crack tip and its wake, the CuZnAl single crystal exhibits significant non-symmetric transformation zones. This phenomenon can be attributed to the high elastic anisotropy at the vicinity of the crack tips that nucleate different martensite variants. In the case of [143] CuZnAl, we found the activation of V2 and V17 martensite variants that match the crystallographic theory and that define the geometry of the transformation domain.

(ii) The stress intensity associated with the asymmetric transformation is numerically determined in this study using an anisotropic elasticity-micro-mechanical calculation. We unveil a deshielding mechanism (positive Mode I and Mode II components) due to such asymmetric transformation at the crack tip which promotes fatigue crack growth. The high levels of local Mode I and II stress intensities reduce the allowable external stress magnitude resulting in lower design stresses. The handbook solution for the calculated stress intensity modified with internal K change matches the

regression results derived from measured displacements very closely lending considerable credibility to our approach.

(iii) A successful regression fitting between experimental displacement fields and analytical solutions is revealed. Although the intrinsic level of threshold stress intensity factor for superelastic [143] CuZnAl single crystal is of the order of 4.5 MPa $m^{1/2}$, the extrinsic level is only 2 MPa $m^{1/2}$ which is a dramatic reduction.

Acknowledgement

This work is funded by the National Science Foundation DMR grant 1709515 Metallic Materials and Nanomaterials Program. The EBSD and TEM analyses were carried out in part in the Frederick Seitz Materials Research Laboratory Central Research Facilities, University of Illinois.

Appendix. The calculation of weight functions

The definition of weight function dates back to Bueckner [34] and Rice [24]. Essentially, the derivation of the weight functions can be achieved by solving the following equations if the crack tip horizontal ($u^{(1)}$), vertical ($v^{(1)}$) displacement fields and K values in a reference loading system (1) are known,

$$h_x = \frac{H}{2K_{(1)}}\frac{du^{(1)}}{dl} \tag{A1a}$$

$$h_y = \frac{H}{2K_{(1)}}\frac{dv^{(1)}}{dl} \tag{A1b}$$

where l denotes the length of the crack and H is an appropriate elastic modulus: for anisotropic materials the modulus can be chosen from the work of Sih et al. [41], which will be elaborated later in this section. Equation (A1) was conveniently written in cartesian coordinate. However, the transformation from cartesian to cylindrical coordinate is feasible and has been illustrated in Ref. [16].

Due to the inclined nature of the crack propagation in [143] CuZnAl single crystal, both Mode I and Mode II stress intensities exist. In other words, we can have weight functions in Mode I and Mode II due to the displacements in x' and y' directions, i.e. $h_{Ix'}$, $h_{IIx'}$,$h_{Iy'}$and $h_{IIy'}$ (see Fig. 6 for the definition of x' and y'), as well. These terms are given in Equation (A2) in cylindrical coordinates,

$$h_{Ix'} = \frac{H}{2K_1}\left(\frac{du^{I}}{d\theta}\frac{\sin\theta}{r} - \frac{du^{I}}{dr}\cos\theta\right) \tag{A2a}$$

$$h_{IIx'} = \frac{H}{2K_2}\left(\frac{du^{II}}{d\theta}\frac{\sin\theta}{r} - \frac{du^{II}}{dr}\cos\theta\right) \tag{A2b}$$

$$h_{Iy'} = \frac{H}{2K_1}\left(\frac{dv^{I}}{d\theta}\frac{\sin\theta}{r} - \frac{dv^{I}}{dr}\cos\theta\right) \tag{A2c}$$

$$h_{IIx'} = \frac{H}{2K_2}\left(\frac{dv^{II}}{d\theta}\frac{\sin\theta}{r} - \frac{dv^{II}}{dr}\cos\theta\right) \tag{A2d}$$

where the definitions of θ and r are illustrated in Fig. 6. The correlations between the components of the crack tip displacement fields, u^{I}, u^{II}, v^{I} and v^{II}, and the Mode I and Mode II stress intensity factors, K_1 and K_2, have been derived by Sih et al. [41] as follows,

$$u^{I} = K_1\sqrt{2r}\mathrm{Re}\left[\frac{1}{\mu_1-\mu_2}\left(\mu_1 p_2\sqrt{\cos\theta+\mu_2\sin\theta} - \mu_2 p_1\sqrt{\cos\theta+\mu_2\sin\theta}\right)\right] \tag{A3a}$$

$$u^{II} = K_2\sqrt{2r}\mathrm{Re}\left[\frac{1}{\mu_1-\mu_2}\left(p_2\sqrt{\cos\theta+\mu_2\sin\theta} - p_1\sqrt{\cos\theta+\mu_2\sin\theta}\right)\right] \tag{A3b}$$

$$v^{I} = K_1\sqrt{2r}\mathrm{Re}\left[\frac{1}{\mu_1-\mu_2}\left(\mu_1 q_2\sqrt{\cos\theta+\mu_2\sin\theta} - \mu_2 q_1\sqrt{\cos\theta+\mu_2\sin\theta}\right)\right] \tag{A3c}$$

$$v^{II} = K_2\sqrt{2r}\mathrm{Re}\left[\frac{1}{\mu_1-\mu_2}\left(q_2\sqrt{\cos\theta+\mu_2\sin\theta} - q_1\sqrt{\cos\theta+\mu_2\sin\theta}\right)\right] \tag{A3d}$$

where μ_1 and μ_2 are the roots of Equation (A4) where a_{11}, a_{22}, a_{12}, a_{16} and a_{66} are the compliance of elastic constants for CuZnAl [42] and p_i and q_j are the anisotropic terms defined in Equation (A5).

$$a_{11}\mu^4 - 2a_{16}\mu^3 + (2a_{12}+a_{66})\mu^2 - 2a_{26}\mu + a_{22} = 0 \tag{A4}$$

$$p_i = a_{11}\mu_i^2 + a_{12} - a_{16}\mu_i \tag{A5a}$$

$$q_j = a_{12}\mu_j + \frac{a_{22}}{\mu_j} - a_{26} \tag{A5b}$$

Sih et al. [41] also provided the solutions for the Mode I and Mode II stress intensity factors in an anisotropic media. In particular, they calculated the K_1 and K_2 values due to the traction fields over the crack surface (Zone 4 in Fig. 6). These solutions are presented in Equation (A6) as the reference loading system (where a solution is known) and the elastic moduli, H, of an anisotropic case were given as expressed in Equation (A7),

$$K_1 = -\frac{1}{\pi\sqrt{a}}\int_0^a t_{y'}(x')\left[\sqrt{\frac{a+x}{a-x}} - \frac{1}{2}\frac{\alpha_o}{\beta_o}\right]dx' \tag{A6a}$$

$$K_2 = -\frac{1}{\pi\sqrt{a}}\int_0^a t_{x'}(x')\left\{\frac{\alpha_o^2}{2\beta_o} + \frac{1}{2\beta_o}\left[\frac{a_{12}}{a_{11}} + \left(\alpha_o^2+\beta_o^2\right)\right]\right\}dx' \tag{A6b}$$

$$H = -\frac{1}{8}\left(\frac{\mu_1-\mu_2}{\mu_2}\right)\left\{\frac{i}{\alpha_o\beta_o}\left[\frac{a_{12}}{a_{11}} + \left(\alpha_o^2-\beta_o^2\right)\right] + 1\right\} \tag{A7}$$

where α_o and β_o are the real and imaginary part of the μ terms, i.e. $\mu_1 = \alpha_o + \beta_o i$ and $\mu_2 = -\alpha_o + \beta_o i$.

References

[1] K. Otsuka, C.M. Wayman, Shape Memory Materials, Cambridge university press, 1999.

[2] T.W. Duerig, K. Melton, D. Stöckel, Engineering Aspects of Shape Memory Alloys, Butterworth-Heinemann, 2013.

[3] K. Melton, O. Mercier, Fatigue of NiTi thermoelastic martensites, Acta Metall. 27 (1979) 137–144.

[4] P. Chowdhury, H. Sehitoglu, Mechanisms of fatigue crack growth – a critical digest of theoretical developments, Fatigue Fract. Eng. Mater. Struct. 39 (2016)

652–674.
[5] A.L. McKelvey, R.O. Ritchie, Fatigue-crack growth behavior in the superelastic and shape-memory alloy nitinol, Metall. Mater. Trans. A 32 (2001) 731–743.
[6] K. Gall, J. Tyber, G. Wilkesanders, S.W. Robertson, R.O. Ritchie, H.J. Maier, Effect of microstructure on the fatigue of hot-rolled and cold-drawn NiTi shape memory alloys, Mater. Sci. Eng.: A 486 (2008) 389–403.
[7] R.O. Ritchie, Near-threshold fatigue-crack propagation in steels, Int. Met. Rev. 24 (1979) 205–230.
[8] A.L. McKelvey, R.O. Ritchie, Fatigue-crack Propagation in Nitinol, a Shape-Memory and Superelastic Endovascular Stent Material, vol. 47, 1999, pp. 301–308.
[9] P. Chowdhury, H. Sehitoglu, A revisit to atomistic rationale for slip in shape memory alloys, Prog. Mater. Sci. 85 (2017) 1–42.
[10] S. Alkan, H. Sehitoglu, Prediction of transformation stresses in NiTi shape memory alloy, Acta Mater. 175 (2019) 192–195.
[11] G.M. Vasko, P.H. Leo, T.W. Shield, Prediction and observation of crack tip microstructure in shape memory CuAlNi single crystals, J. Mech. Phys. Solids 50 (2002) 1843–1867.
[12] G.M. Loughran, T.W. Shield, P.H. Leo, Fracture of shape memory CuAlNi single crystals, Int. J. Solids Struct. 40 (2003) 271–294.
[13] E. Sgambitterra, C. Maletta, F. Furgiuele, H. Sehitoglu, Fatigue crack propagation in [0 1 2] NiTi single crystal alloy, Int. J. Fatigue 112 (2018) 9–20.
[14] R. McMeeking, A. Evans, Mechanics of transformation-toughening in brittle materials, J. Am. Ceram. Soc. 65 (1982) 242–246.
[15] K. Gall, K. Jacobus, H. Sehitoglu, H.J. Maier, Stress-induced martensitic phase transformations in polycrystalline CuZnAl shape memory alloys under different stress states, Metall. Mater. Trans. A 29 (1998) 765–773.
[16] Y. Wu, A. Ojha, L. Patriarca, H. Sehitoglu, Fatigue crack growth fundamentals in shape memory alloys, Shape Memory and Superelasticity 1 (2015) 18–40.
[17] H. Tada, P. Paris, G. Irwin, The Analysis of Cracks Handbook, vol. 2, ASME Press, New York, 2000, p. 1.
[18] R.O. Ritchie, Mechanisms of fatigue crack propagation in metals, ceramics and composites: role of crack tip shielding, Materials Science and Engineering: A 103 (1988) 15–28.
[19] S. Suresh, Fatigue of Materials, Cambridge university press, 1998.
[20] S. McNeill, W. Peters, M. Sutton, Estimation of stress intensity factor by digital image correlation, Eng. Fract. Mech. 28 (1987) 101–112.
[21] J. Carroll, C. Efstathiou, J. Lambros, H. Sehitoglu, B. Hauber, S. Spottswood, et al., Investigation of fatigue crack closure using multiscale image correlation experiments, Eng. Fract. Mech. 76 (2009) 2384–2398.
[22] G.J. Pataky, M.D. Sangid, H. Sehitoglu, R.F. Hamilton, H.J. Maier, P. Sofronis, Full field measurements of anisotropic stress intensity factor ranges in fatigue, Eng. Fract. Mech. 94 (2012) 13–28.
[23] J.D. Eshelby, The determination of the elastic field of an ellipsoidal inclusion, and related problems, Proc. Roy. Soc. Lond. Series A Math. Phys. Sci. 241 (1957) 376–396.
[24] J.R. Rice, Some remarks on elastic crack-tip stress fields, Int. J. Solids Struct. 8 (1972) 751–758.
[25] W.S. LePage, A. Ahadi, W.C. Lenthe, Q.-P. Sun, T.M. Pollock, J.A. Shaw, et al., Grain size effects on NiTi shape memory alloy fatigue crack growth, J. Mater. Res. 33 (2017) 91–107.
[26] R. Vaidyanathan, D. Dunand, U. Ramamurty, Fatigue crack-growth in shape-memory NiTi and NiTi–TiC composites, Mater. Sci. Eng.: A 289 (2000) 208–216.
[27] T. Chu, W. Ranson, M.A. Sutton, Applications of digital-image-correlation techniques to experimental mechanics, Exp. Mech. 25 (1985) 232–244.
[28] E. Patoor, M. El Amrani, A. Eberhardt, M. Berveiller, Determination of the origin for the dissymmetry observed between tensile and compression tests on shape memory alloys, J. Phys. IV 5 (1995). C2-495-C2-500.
[29] S. Chakravorty, C. Wayman, Electron microscopy of internally faulted Cu-Zn-Al martensite, Acta Metall. 25 (1977) 989–1000.
[30] J. Perkins, W. Muesing, Martensitic transformation cycling effects in Cu-Zn-Al shape memory alloys, Metall. Trans. A 14 (1983) 33–36.
[31] G. Firstov, J. Van Humbeeck, Y.N. Koval, High temperature shape memory alloys problems and prospects, J. Intell. Mater. Syst. Struct. 17 (2006) 1041–1047.
[32] T. Mura, Micromechanics of Defects in Solids, Springer Science & Business Media, 2013.
[33] S. Yi, S. Gao, L. Shen, Fracture toughening mechanism of shape memory alloys under mixed-mode loading due to martensite transformation, Int. J. Solids Struct. 38 (2001) 4463–4476.
[34] H. Bueckner, Novel principle for the computation of stress intensity factors, Zeitschrift fuer Angewandte Mathematik & Mechanik (1970) 50.
[35] K. Tanaka, Fatigue crack propagation from a crack inclined to the cyclic tensile axis, Eng. Fract. Mech. 6 (1974) 493–507.
[36] S. Dilibal, H. Sehitoglu, R. Hamilton, H. Maier, Y. Chumlyakov, On the volume change in Co–Ni–Al during pseudoelasticity, Mater. Sci. Eng.: A 528 (2011) 2875–2881.
[37] W. Abuzaid, H. Sehitoglu, Shape memory effect in FeMnNiAl iron-based shape memory alloy, Scripta Mater. 169 (2019) 57–60.
[38] C. Efstathiou, H. Sehitoglu, Local transformation strain measurements in precipitated NiTi single crystals, Scripta Mater. 59 (2008) 1263–1266.
[39] M. Nishida, H. Ohgi, I. Itai, A. Chiba, K. Yamauchi, Electron microscopy studies of twin morphologies in B19′ martensite in the Ti-Ni shape memory alloy, Acta Metall. Mater. 43 (1995) 1219–1227.
[40] S. Alkan, Y. Wu, H. Sehitoglu, Giant non-Schmid effect in NiTi, Extreme Mech. Lett. 15 (2017) 38–43.
[41] G.C. Sih, P. Paris, G.R. Irwin, On cracks in rectilinearly anisotropic bodies, Int. J. Fract. Mech. 1 (1965) 189–203.
[42] B. Verlinden, T. Suzuki, L. Delaey, G. Guenin, Third order elastic constants of β CuZnAl as a function of the temperature, Scripta Metall. 18 (1984) 975–979.
[43] J. Yaacoub, Y. Wu, W. Abuzaid, D. Canadinc, H. Sehitoglu, Martensite variant localization effects on fatigue crack growth – the cuznal example, Scripta Mat. (2019) article in press, https://doi.org/10.1016/j.scriptamat.2019.06.032.